

# Study of Magnetic Field Effects in Drift Tubes for the Barrel Muon Chambers of the CMS Detector at the LHC

M. Aguilar-Benítez<sup>a</sup>, M. Arneodo<sup>b</sup>, M. Benettoni<sup>c</sup>,  
A. Benvenuti<sup>d</sup>, J. Berdugo<sup>a</sup>, S. Bethke<sup>e</sup>, M. Cerrada<sup>a</sup>,  
R. Cirio<sup>b</sup>, N. Colino<sup>a</sup>, F. Conti<sup>c</sup>, M. Dallavalle<sup>d</sup>, M. Daniel<sup>a</sup>,  
F. Daudo<sup>b</sup>, M. De Giorgi<sup>c</sup>, A. De Min<sup>c</sup>, U. Dosselli<sup>c</sup>,  
C. Fanin<sup>c</sup>, B. Fehr<sup>e</sup>, M.C. Fouz<sup>a</sup>, F. Gasparini<sup>c</sup>, U. Gasparini<sup>c</sup>,  
R. Giantin<sup>c</sup>, V. Giordano<sup>d</sup>, P. Guaita<sup>c</sup>, M. Guerzoni<sup>d</sup>,  
I. Lippi<sup>c</sup>, P. Ladrón de Guevara<sup>a</sup>, S. Marcellini<sup>d</sup>, F. Martín<sup>a</sup>,  
R. Martinelli<sup>c</sup>, S. Maselli<sup>b</sup>, A. Meneguzzo<sup>c</sup>, E. Migliori<sup>b</sup>,  
J. Mocholí<sup>a</sup>, A. Montanari<sup>d</sup>, F.L. Navarria<sup>d</sup>, F. Odorici<sup>d</sup>,  
M. Pegoraro<sup>c</sup>, C. Peroni<sup>b</sup>, H. Reithler<sup>e</sup>, L. Romero<sup>a</sup>,  
A. Romero<sup>b</sup>, P. Ronchese<sup>c</sup>, A.M. Rossi<sup>d</sup>, T. Rovelli<sup>d</sup>,  
A.J. Sancho<sup>c</sup>, P. Sartori<sup>c</sup>, H. Schwarthoff<sup>e</sup>, V. Sondermann<sup>e</sup>,  
A. Staiano<sup>b</sup>, V. Tano<sup>e</sup>, H. Teykal<sup>e</sup>, E. Torassa<sup>c</sup>, J. Tutas<sup>e</sup>,  
J. Vandenhirtz<sup>e</sup>, H. Wagner<sup>e</sup>, M. Wegner<sup>e</sup>, C. Willmott<sup>a</sup>,  
P. Zotto<sup>c</sup>, G. Zumerle<sup>c</sup>

<sup>a</sup> CIEMAT - División de Física de Partículas, Madrid, Spain

<sup>b</sup> Univ. di Torino e Sez. dell' INFN, Torino, Italy

<sup>c</sup> Univ. di Padova e Sez. dell' INFN, Padova, Italy

<sup>d</sup> Univ. di Bologna e Sez. dell' INFN, Bologna, Italy

<sup>e</sup> III. Physikalisches Institut der RWTH Aachen, Germany

---

## Abstract

The drift chambers in the barrel region of the CMS detector are exposed to magnetic stray fields. To study the performance of the muon reconstruction and the drift time based muon trigger, prototypes were tested under the expected magnetic field conditions at the H2 test facility at CERN. The results indicate that the overall chamber performance will not be affected. Only the bunch crossing identification capability in the small region near  $\eta = 1.1$ , corresponding to the border of the solid angle region covered by the barrel, will be weakened.

---

## 1 Introduction

The design goals of the barrel CMS drift chambers include muon identification, track reconstruction and trigger capabilities [1]. The muon trigger is based on a so called Mean Timing technique [2,3]. It requires a homogeneous drift velocity as well as an adequate time resolution in order to resolve the proton bunch crossing frequency of 25 ns at the LHC. Results from prototypes with an optimised drift cell design, in the absence of magnetic field, have been recently presented [4]. They show that the requirements for the muon reconstruction and triggering in the barrel muon system of CMS can be met. The selected drift gas, Ar:CO<sub>2</sub> (85:15) under normal conditions, is a compromise of low cost, low ageing propensity, and sufficient quenching ability with fast saturation. The drift cell design ensures a homogeneous electric field of approximately 2 kV/cm except in the regions close to the anode and the cathode.

In CMS the barrel muon chambers will be exposed to magnetic stray fields varying in orientation and magnitude along the chamber volume. Assuming a 4 T field inside the solenoid, stray fields in the chambers are expected to remain well below 0.4 T with the exception of a small region where it can go up to 0.8 T. Under the influence of crossed electric and magnetic fields the large Lorentz angle of the gas will reduce the effective drift velocity. Provided that the magnetic field is known in orientation and magnitude, corrections can be applied during offline muon track reconstruction. At trigger level however, large variations of the magnetic field along the anode wires cannot be corrected for.

In order to quantify the magnetic field effects on the Mean Timing procedure, and on the chamber performances, measurements were carried out with drift chamber prototypes at the H2 test beam area at CERN. The results obtained are presented in this paper.

## 2 The Barrel Muon System

The central muon system of the CMS detector [1] consists of four muon stations (MB1, MB2, MB3 and MB4) placed inside the iron return yoke of a superconducting solenoidal magnet as shown in fig. 1. It is built up by five concentric rings enclosing the coil and the inner detectors.

The central and adjacent rings are separated by 15 cm (space needed for the cabling of the subdetectors and the cryogenic support system). Separation distances in between the outer rings are 12 cm.

In the transverse view the muon stations are divided in 12 sectors, thus each covering an angle range of  $30^\circ$ . In each muon station the bending of the muon track in the transverse projection is measured in two groups of 4 layers of drift tubes ( $\phi$  layers). Another group of four layers ( $\theta$  layers), measure the projection along the proton beam axis. The groups of 4 layers are called quadruplets or superlayers. Adjacent layers in a quadruplet are staggered by half a cell.

The magnet has been designed [7] to provide a homogeneous magnetic field of 4 T parallel to the proton beam axis inside the coil volume. The iron of the yoke is saturated by the returning magnetic field lines with a magnitude close to 1.8 T. The inhomogeneous field lines at the end of the coil and in the gaps between the return yoke rings are leaking into the four muon stations. In average the magnetic field has a good symmetry around the beam line axis. Their components perpendicular ( $B_r$ ) and parallel ( $B_z$ ) to the proton beam axis are shown in fig. 2.

The parallel component  $B_z$  stays approximately constant in each of the muon stations and is rarely larger than 0.2 T. It rises up to 0.3 or 0.4 T only in the last centimeters of the chambers (this space is partly used for mechanical support of the wires and for electrical connections).

The strongest variations in the radial magnetic field component  $B_r$  are in the forward ring. There  $B_r$  varies from 0.2 to 0.8 T along the station MB1. In MB2 it reaches a value close to 0.35 T but stays approximately constant. In MB4 the sign of the magnetic field component changes, although its absolute value does not get larger than 0.2 T. A similar behaviour holds for MB4 in the middle ring. In all the other stations the magnetic field stays always below 0.2 T.

## 2.1 Magnetic Field Effects

In the case of crossed magnetic and electric fields the drift of electrons is influenced by the Lorentz force according to the expression

$$\mathbf{v}_{drift} = \frac{e}{m_e} \tau |\mathbf{E}| \frac{1}{1 + (\omega\tau)^2} (\tilde{\mathbf{E}} + \omega\tau[\tilde{\mathbf{E}} \times \tilde{\mathbf{B}}] + (\omega\tau)^2(\tilde{\mathbf{E}}\tilde{\mathbf{B}})\tilde{\mathbf{B}}) \quad (1)$$

with  $m_e$ ,  $e^-$  mass and charge of the electron,  $\omega$  the cyclotron frequency,  $\tau$  the electron collision frequency and  $\tilde{\mathbf{E}}$ ,  $\tilde{\mathbf{B}}$  the normal field vectors (see e.g. [8]). If fields are orthogonal, the drift velocity can be simply parametrized as

$$v_{drift}(E, B) = v_{drift}(E, 0) \cos(\alpha_L(E, B)) \quad (2)$$

with  $\alpha_L$  the Lorentz angle. The value of  $\alpha_L$  depends on the electric and magnetic field strength and must be measured for any drift gas mixture.

In Ar:CO<sub>2</sub>(85:15) one measures for an electric field strength of 2 kV/cm a Lorentz angle of 12° for  $B = 0.5$  T and 18° for  $B = 0.83$  T [6]. This would translate into an increase of the maximum drift time in the drift tubes of approximately 8 ns and 18 ns, respectively.

In the quadruplet local reference system, we call the three components of the magnetic field  $B_N$ ,  $B_W$  and  $B_E$ . The first one,  $B_N$ , is orthogonal to the plane defined by the wires in one layer, and also to the electric field. The other two components,  $B_W$  and  $B_E$ , stay inside the wire plane: the former one is parallel to the wires and the latter one is parallel to the electric field.

In the simple picture of expression (1), neglecting anisotropic diffusion,  $B_E$  would not affect the drift velocity significantly. Therefore, the main effects should come mainly from the components  $B_W$  and  $B_N$ . In particular  $B_W$  would distort the drift electron trajectories as shown in fig. 3, whereas  $B_N$  would introduce a longer drift path towards the anode, as sketched in fig. 4.

Naively one should expect that the only effect of  $B_N$  is to change the effective drift velocity. In the case of  $B_W$ , distortions of the drift lines may, in addition, produce inefficiencies, because of decreasing the active cell volume, and may also affect the symmetry of the behaviour of the cell with respect to the angle of incidence.

We have measured the influence of each of these three components of the B field using small size prototypes in a test beam at CERN during 1995 and 1996. From this study we can calculate the magnetic field effects to be expected in each of the  $\phi$  and  $\theta$  layers of the final CMS barrel muon detector. In particular,  $\phi$  layers will be exposed to magnetic field components  $B_N = B_r \cos \Phi$ ,  $B_E = B_r \sin \Phi$  and  $B_W = B_z$ , whereas in the case of  $\theta$  layers  $B_N = B_r \cos \Phi$ ,  $B_E = B_z$  and  $B_W = B_r \sin \Phi$ ,  $\Phi$  ranging approximately from -15° to 15°.

### 3 Experimental Setup

Several prototypes were installed inside the superconducting magnet M2 of the H2 test beam facility at CERN. Their main features were described in [4]. All of them had in common the drift cell configuration of fig. 3 and consisted of at least one quadruplet. Data were taken in two periods with different orientations of the magnetic field with respect to the muon beam direction:

- During 1995 the magnetic field was parallel to the incoming muon beam. This configuration is ideal to study  $B_N$ . Prototype chambers were placed orthogonal to the beam with anode wires in a vertical direction. A tilt of the chamber around a horizontal axis allowed to study combined  $B_N$  and  $B_W$  effects.
- During 1996 the magnetic field was in a horizontal direction perpendicular to the beam. Superlayers with anode wires in a vertical direction were used to measure  $B_E$  effects, whereas superlayers with horizontal anode wires provided information on the influence of  $B_W$ .

Incoming muons had a momentum in the range 200 to 300 GeV/ $c$ . The setup allowed to rotate the chamber prototypes around an axis parallel or orthogonal to the anode wires in order to study the effects of different angles of incidence. All prototypes were operating with the drift gas Ar:CO<sub>2</sub>(85:15) under normal conditions. As indicated in fig. 3, the voltages used were 3.6/1.8/-1.8 kV on anode/electrode/cathode (reference voltages in [4]). A significant fraction of the data was also taken with voltage settings at 3.3/1.5/-1.5 kV. The gain, controlled by the difference between the anode and electrode voltages, is similar in both cases but the second setting provides a lower drift field as a consequence of the smaller voltage difference between electrode and cathode.

## 4 Performance under $B_E$ and $B_W$

### 4.1 Drift Velocity and Linearity

The so called “mean time” obtained from three consecutive layers, staggered half a cell, according to

$$t_{MT} = \frac{1}{2}(t_j + t_{j+2}) + t_{j+1} = t_{drift}^{max} \quad (3)$$

provides a measurement of the maximum drift time, and hence of the drift velocity if a linear space-time relation is assumed. We present in fig. 5 the results obtained for the drift velocity at several values of the magnetic field. As expected, fig. 5 shows no significant change of the drift velocity as a function of the magnetic field value  $B_E$ . On the other hand, there is a clear effect in the case of  $B_W$ , the effective drift velocity decreasing as  $B_W$  increases. The effect is small (of the order of 1 %) at  $B_W = 0.4$  T, and becomes very important at high  $B_W$  values ( greater than 5 % at  $B_W = 1$  T).

High  $B_W$  field values are also expected to affect the linearity of the space-time relation. Distortions should appear mainly in the region near the cathode I

beams. Evidence for these distortions can be found in the distributions of the residuals from a track fit assuming a constant drift velocity. The average values of these fit residual distributions as a function of the distance to the wire calculated in 1 mm bin slices is shown in fig. 6 for two values of  $B_W$ . In the case of  $B_W = 0.8$  T, linearity is quite good in the central region of the cell. However, it becomes much worse in the last few mm close to I beams where deviations from linearity become larger than 0.5 mm (because of the geometry of staggered adjacent layers, effects near the wire and near the I beams are strongly correlated). On the other hand, as also shown in fig. 6, there are no significant deviations from linearity if  $B_W$  stays below 0.2 T, which will be the case in CMS.

#### 4.2 Resolution

The width of the  $t_{MT}$  variables provide an estimate of the single wire resolution. We show in fig. 7 the effect of the magnetic field on this resolution value. Again, no dependence can be seen when  $B$  is parallel to the electric field. However, for  $B$  parallel to the wire, resolution gets clearly worse when the magnetic field increases. From fig. 7 one can see that for  $B_W$  values smaller than 0.4 T, the resolution is always better than 250 microns which is an acceptable value. Since  $B_W$  will never exceed 0.4 T in the active volume of the chambers at CMS, one can conclude that the effect of the component of the magnetic field along the wire on the resolution will not be a problem.

#### 4.3 Efficiency

Tracks having 3 and 4 hits in the quadruplet are used to calculate the single wire efficiency. In fig. 8 a drop in efficiency for high values of  $B_W$  can be seen. Qualitatively this effect was expected from simulations. The distortion of the drift lines shown in fig. 3 becomes bigger as  $B_W$  increases and it could eventually produce a hole in the acceptance for muon tracks going through the first few millimeters away from the cathode I beams. This can be better seen in fig. 9 which shows the efficiency as a function of the distance to the wire for several values of  $B_W$ . Below 0.4 T, the efficiency is still high in the whole drift volume.

On the other hand, as also shown in fig. 8, variations on  $B_E$  do not affect chamber efficiency in a significant way.

As indicated in fig. 3, the effect of  $B_W$  on the drift lines can be seen as a rotation of the tube around its wire. This affects the symmetry of the behaviour of the cell with respect to tracks which have positive or negative angles compared to normal incidence. The effect can be simulated by taking data at a given angle of incidence with positive and negative magnetic field.

In fig. 10 the maximum drift time is shown as a function of  $B_W$  for several angles of incidence. Asymmetry effects are clearly visible. One can see in fig. 10 that even at  $B = 0$  the maximum drift time is affected by the track angle of incidence as previously observed [4]. From  $0^\circ$  to  $24^\circ$ , this variation amounts to 7 ns. In the presence of a magnetic field of 0.1 T parallel to the wires, the variation of the maximum drift time from  $-24^\circ$  to  $24^\circ$  is increased to approximately 12 ns. Most of the high  $p_T$  muon tracks traversing the CMS barrel chambers will stay inside this angular range. Bunch crossing identification puts a constraint on the acceptable maximum drift time variation. Basically it should never exceed the interbunch time of 25 ns in order to avoid inefficiencies of the trigger algorithm. Therefore asymmetry effects, although non negligible, are expected to have a minor influence on the drift chamber trigger capability at CMS.

## 5 Performance under $B_N$

### 5.1 Drift Velocity and Linearity

The simulated effect of a magnetic field component  $B_N = 1$  T on the electron drift in the drift tubes is shown in fig. 11. Up to a drift distance of 2 mm the electric field is very high. Therefore, the magnetic field deflection is small and the drift velocity stays essentially unchanged.

For drift distances greater than 2 mm the drift velocity is constant to a good approximation. This reflects the small variations of the Lorentz angle at the given range of the electric field strength of  $(2.3 \pm 0.3)$  kV/cm for the nominal voltages. In table 1 the average drift velocity, the corresponding maximum drift time and the Lorentz angle are shown for two voltages and magnetic field settings.

Table 1 shows that with nominal high voltage settings the value of  $t_{MT}$  increases by 27 ns when going from  $B_N = 0$  to  $B_N = 1$  T. This is certainly a very important effect which, if not corrected for, would spoil bunch crossing

identification at the trigger level. In section 6 we will discuss the implications of this effect in the chamber performance at the expected working conditions of the CMS experiment.

The mean time defined in (3) is expected to be independent of the incident angle and the track position in the drift cell for a constant drift velocity. This is fulfilled to a good approximation in the magnetic field-less case, as shown for example in fig. 12 for perpendicular tracks. This figure also shows that at  $B_N = 1.0$  T the presence of non linearities is quite clear (they could be of the order of 250 or 300 microns at most since the mean time value stays within a range of  $\pm 5$  ns the average of  $t_{MT}$ ). Even if the effect of the reduced effective drift velocity is properly taken into account, in the case of  $B_N = 1$  T the fraction of muon tracks which are within  $(t_{MT} \pm 12.5)$ ns decreases by 5% when compared to the situation at  $B_N = 0$  because of the non linearities.

### 5.2 Resolution

In fig. 13 the dependence of the single wire resolution with the magnetic field component  $B_N$  is shown. The plot includes several angles of incidence to take account of the range covered by  $\phi$  layers in CMS. It shows that once the proper effective drift velocity is taken into account there is no sizable degradation of the average spatial resolution. At  $B_N = 1$  T the resolution gets near to 280 microns, which is still within the design goals for the drift tube chambers.

### 5.3 Efficiency

The single wire efficiency, calculated in the drift volume, is shown in fig. 14. Also in this case the influence of having different angles of incidence was studied. At all  $B_N$  values, even at 1 T, efficiency is always bigger than 99% for the whole angular region measured.

## 6 Performance under $B_N$ and $B_W$

The effect of combining the two magnetic field components,  $B_N$  and  $B_W$ , on the mean timing performance is shown in fig. 15 for the case  $B_N = 0.9$  T and  $B_W = 0.45$  T. The comparison with fig. 12, and with the results presented in section 4.1, show that  $B_W$  is responsible for the strong degradation in the linearity of the space-time relationship in the vicinity of the cathodes. Excluding these regions the resolution amounts to 235  $\mu$ m.

## 7 Implications for operation at CMS

The most demanding restrictions on the resolution and timing properties apply to the drift tubes of the  $p_T$  measuring  $\phi$ -layers in the barrel muon chambers.

The good homogeneity of the electric field and its high field strength makes the drift tubes insensitive to values of  $B_E$  up to 1 T.

As far as  $B_N$  is concerned, the results demonstrate that both efficiency and resolution measured up to 1 T stay well within the design goals. A more detailed discussion is necessary for the drift velocity and for absolute timing measurements. In each group of four layers inside the same quadruplet the Mean Timing electronics identifies the bunch crossing to which the particle belongs with a fixed delay equal to the maximum drift time. To operate properly the circuit must be tuned to the effective drift velocity. A time window is opened by the Bunch Crossing clock centered at the corresponding maximum drift time and having a width large enough to account for the different time of flight and for the propagation time of the signals along the wire. Therefore, the increase in the maximum drift time produced by the presence of the magnetic field can be properly taken into account by increasing accordingly the time delay of the window in steps of one nanosecond. This tuning would be fully effective if the field is uniform along the wire length. A non uniform field however generates an additional dispersion on the maximum drift time. Corrections can of course be applied in the offline analysis in order to account for the magnetic field variation. Field uncertainties of 5% would introduce maximum errors comparable to the drift tube resolution at 1 T and negligible errors below 0.5 T. Obviously this cannot be applied at the trigger level. Trigger capability is affected differently in different chambers.

In MB2 to MB4 the normal component  $B_N$  yields values which are less than 0.4 T. The influence of the increase of the maximal drift time at  $B_N = 0.5$  T by 5 ns on the mean timing efficiency is moderate, as can be estimated from the taken data even without a detailed simulation of the trigger electronics implementation. By simply taking a time window of 25 ns around the maximum drift time at  $B_N = 0$  T, we find that the fraction of muon tracks in a single triplet of drift cells at  $B_N = 0.5$  T which fall in that window decreases by 8% with respect to the reference drift time. In an optimized time window the mean timing efficiency decreases by 1% for muon tracks at 0 T and 5% at 0.5 T.

In MB1 in the outer wheels however,  $B_N$  rises from 0.2 to 0.8 T along the anode wires. Repeating the same exercise with the data taken at  $B_N=0.5$  T and  $B_N=1.0$  T we find that if the time window is set for  $B=0.5$  T values, the mean timing efficiency would decrease by 8% for muon tracks at  $B=0$  and by

as much as 50% for muon tracks at  $B=1.0$  T. This indicates that a degradation of the capability of an unambiguous Bunch Crossing identification has to be expected in the MB1 chambers near the barrel endcaps in the small region close to  $\eta = 1.1$  (see fig. 1 and fig. 2). To try to reduce this effect by increasing the electric field strength does not help much since the decrease in the Lorentz angle is marginal. Not much can be gained by changing the gas mixture either, because of the boundary conditions ensuring a fast saturated drift gas with low ageing propensity. It should be anyhow stressed that the reported test results apply to the expected performance of one independent superlayer. The global trigger, being determined by at least two muon stations, will help in smoothing out the bad behaviour of critical regions in single superlayers.

In the case of  $B_W$ , the results show that its influence becomes dramatic as the magnetic field value increases. Not only the drift velocity changes very significantly above 0.5 T, but also resolution deteriorates significantly and efficiency losses are very important. It is fortunate that in CMS,  $B_W$  will very rarely exceed 0.2 T, and there the effects will have a minor influence. Only the asymmetries affecting the behaviour of a layer with respect to its normal, as described in section 4.4, should still be taken into consideration when defining the effective drift velocity. The influence of  $B_W$  was already minimized by an improved cell design as described in [10].

## 8 Conclusions

The results shown in this paper confirm that the actual design of drift tubes is adequate to achieve the expected performance in the range of magnetic field values which will be present in the CMS barrel muon detector. Efficiency and resolution are, in all cases, good enough to meet the muon reconstruction and triggering requirements. Minor effects can also be foreseen in the bunch crossing identification capability. Some degradation is only to be expected in the small region of the MB1 chambers close to  $\eta = 1.1$  because of the very high and non uniform radial magnetic field. It is a general conclusion of all the described effects that the trigger processor will have to be carefully optimised taking into account chamber positioning in CMS. Studies of how to implement this have been already done [11] and further work is under way.

## References

- [1] CMS Technical Proposal, CERN/LHCC 94-38, LHCC/P1, 15 December 1994.
- [2] F. Gasparini et al., Nucl. Instr. and Meth. A 336 (1993) 91.
- [3] G. Barichello et al., Nucl. Instr. and Meth. A 360 (1995) 507.
- [4] M. Benettoni et al., Performance of the Drift Tubes for the Barrel Muon Chambers of the CMS Detector at LHC, Nucl. Instr. and Meth. A, in print.
- [5] The CMS Muon Project. Technical Design Report, CERN/LHCC 97-32, 1997.
- [6] Y.-H. Chang et al., Nucl. Instr. and Meth. A 311 (1992) 490.
- [7] The CMS Magnet Project. Technical Design Report, CERN/LHCC 97-10, 1997.
- [8] W. Blum, L. Rolandi, Particle Detection with Drift Chambers, Springer Verlag, Second Printing 1994.
- [9] R. Veenhof, *GARFIELD, a Drift Chamber Simulation Program User's Guide*, Version 5.13, CERN Program Library W5050, 1995.
- [10] A. Benvenuti et al., Simulations in the Development of the Barrel Muon Chambers for the CMS experiment at CERN, Nucl. Instr. and Meth. A, in print.
- [11] M. de Giorgi et al., Nucl. Instr. and Meth. A 398 (1997) 203.

## Table Captions

Table 1: The drift velocity and corresponding maximum drift time and Lorentz angle for different voltage and magnetic field settings.

Table 1

U [kV]	$B_N$ [T]	$t_{drift}^{max}$ [ns]	$\bar{v}_{drift} [\frac{\mu m}{ns}]$	$\alpha_L [^\circ]$
	0	351±2	55,6±0,2	
3.3/1.5/-1.5	0.5	356±2	54,7±0,2	10,4±2
	1.0	394±1	49,5±0,2	26,4±2
	0	346±2	56,4±0,2	
3.6/1.8/-1.8	0.5	351±2	55,7±0,2	9,7±3
	1.0	373±1	52,3±0,2	22,4±1

## Figure Captions

Figure 1: Longitudinal view of a quadrant of the CMS detector showing the position of the 4 barrel muon stations (MB1 to MB4) and also the forward muon system (ME1 to ME4). The interaction point is at the origin of the coordinate system and the proton beams run along the z axis.

Figure 2: The magnetic field components parallel ( $B_z$ ) and perpendicular ( $B_r$ ) to the proton beam axis inside the central muon chambers of the CMS detector. The shaded areas are the gaps between the detector rings shown in fig. 1.

Figure 3: Drift lines in a cell of the CMS barrel muon detector under the influence of a magnetic field of 0.45 T parallel to the anode wires. The drift gas is Ar:CO<sub>2</sub>(85:15). The anode is a 50 micron diameter stainless steel wire. Top and bottom planes are made of 2 mm thick aluminium sheets insulated from aluminium I beam cathodes by Lexan strips 0.5 mm thick. Two copper strip electrodes 14 mm wide, mylar backed for insulation purposes, improve field uniformity.

Figure 4: Drift lines inside the cell in absence of magnetic field are shown in a). The presence of a magnetic field orthogonal to the chamber plane changes the drift direction as shown in b) reflecting in a smaller apparent drift velocity.

Figure 5: Drift velocity as a function of the magnetic field  $B$  in the two configurations:  $B$  parallel to the anode wires ( $B_W$ ), and  $B$  perpendicular to the wires and parallel to the electric field ( $B_E$ ). The chamber was placed orthogonal to the beam.

Figure 6: Mean values of residuals to straight line fits of tracks having hits in all 4 layers of a quadruplet, as a function of the distance to the wire, for data taken with  $B_W = 0.8$  T and  $B_W = 0.18$  T. The former value of  $B_W$  will never be reached in the barrel chambers at CMS. The average values are taken for 1 mm wide slices of distance.

Figure 7: Single wire resolution as a function of the magnetic field  $B$  in the two configurations:  $B$  parallel to the anode wires ( $B_W$ ), and  $B$  perpendicular to the wires and parallel to the electric field ( $B_E$ ).

Figure 8: Efficiency as a function of the magnetic field  $B$  in the two configurations:  $B$  parallel to the anode wires ( $B_W$ ), and  $B$  perpendicular to the wires and parallel to the electric field ( $B_E$ ).

Figure 9: Efficiency as a function of the distance to the wire for different values of  $B_W$ .

Figure 10: Maximum drift time as a function of the magnetic field  $B_W$  for several angles of incidence obtained by rotating the chamber around an axis parallel to the wires. Different values are obtained for positive and negative magnetic fields indicating the asymmetrical behaviour of the drift tube.

Figure 11: The space-time relationship for  $B_N = 0$  T and  $B_N = 1$  T.

Figure 12: The average maximum drift time, calculated from (3), for a triplet of drift cells versus the drift distance in the intermediate cell. The vertical bars are the widths of a Gaussian fit, hence the mean time resolution. The dotted lines indicate an interval of  $\pm 12.5$  ns around the  $B=0$  results corresponding to the proton bunch crossing frequency of 25 ns.

Figure 13: Single wire resolution for several values of the magnetic field component  $B_N$  and of the angle of incidence  $\phi$ .

Figure 14: Average single wire efficiency for several values of the magnetic field component  $B_N$  and of the angle of incidence  $\phi$ .

Figure 15: The average maximum drift time, calculated from (3), for a triplet of drift cells versus the drift distance in the intermediate cell for  $B_N = 0.9$  T and  $B_W = 0.45$  T. These magnetic field values will never be reached in CMS. The vertical bars are the widths of a Gaussian fit. The dotted lines indicate an interval of  $\pm 12.5$  ns corresponding to the proton bunch crossing frequency of 25 ns.

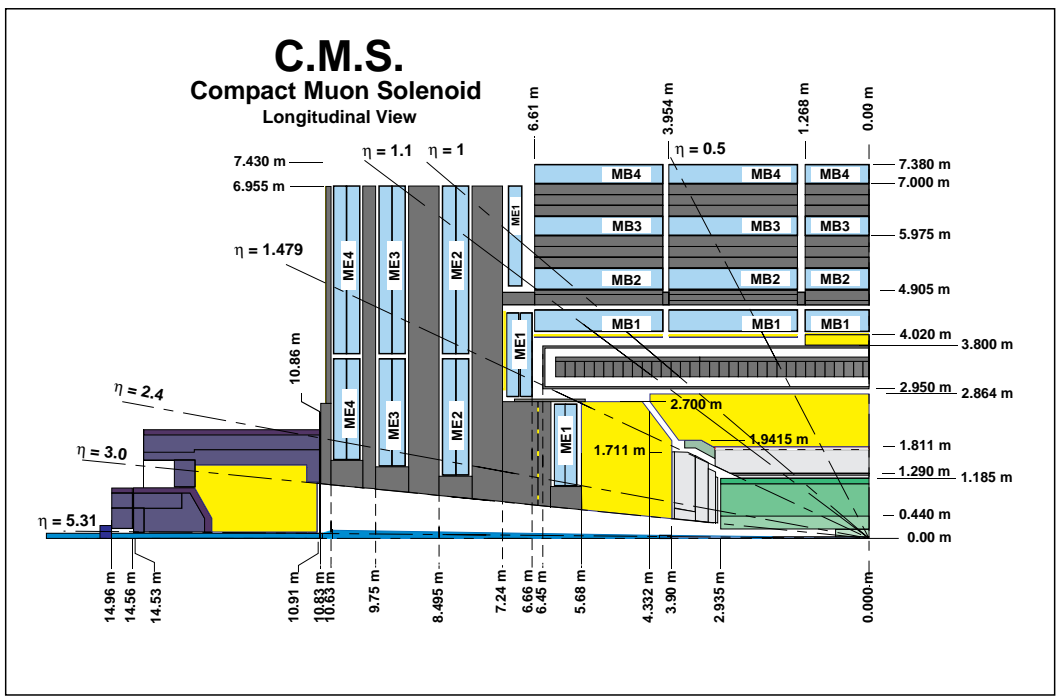


Fig. 1.

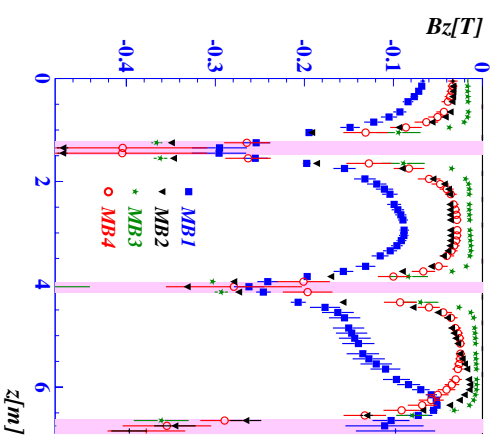
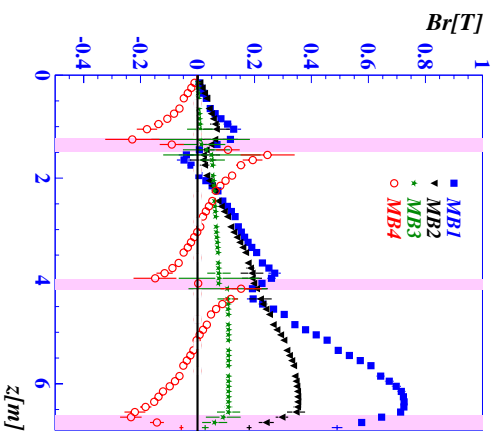


Fig. 2.

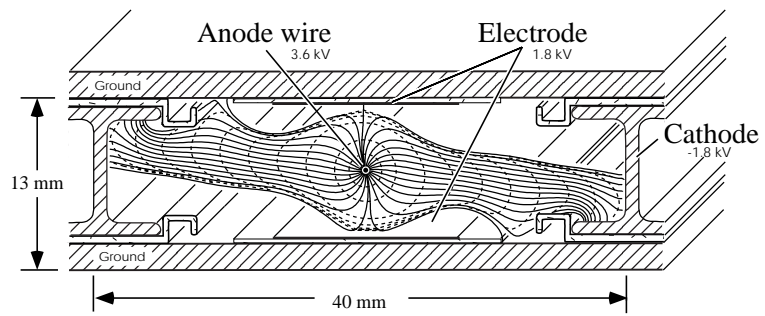


Fig. 3.

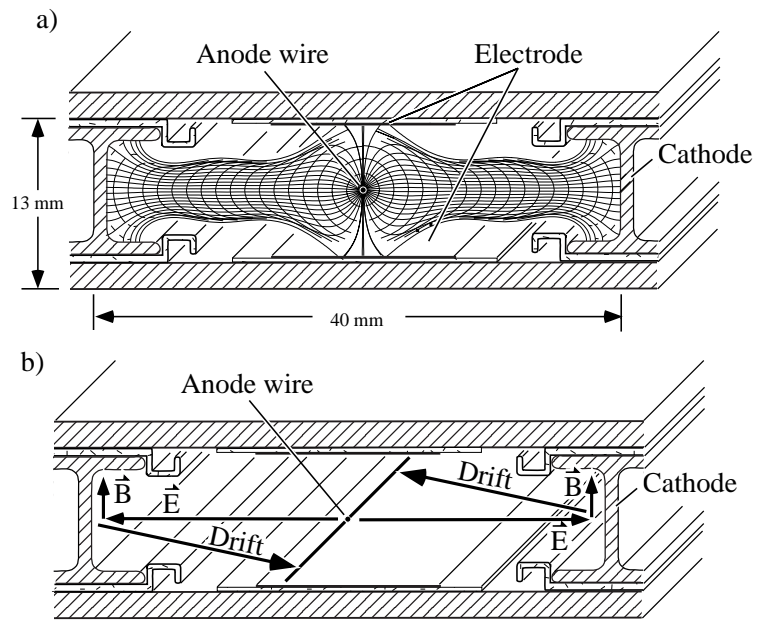


Fig. 4.

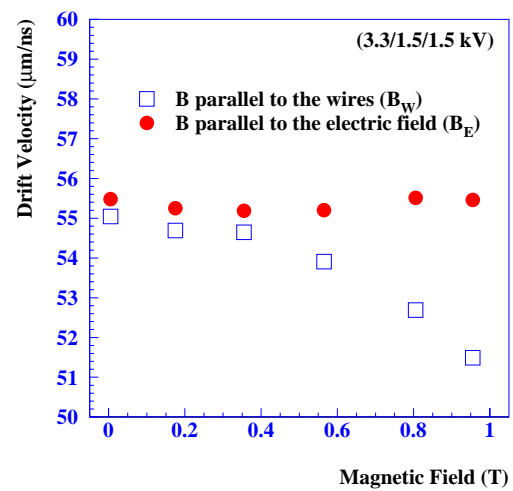


Fig. 5.

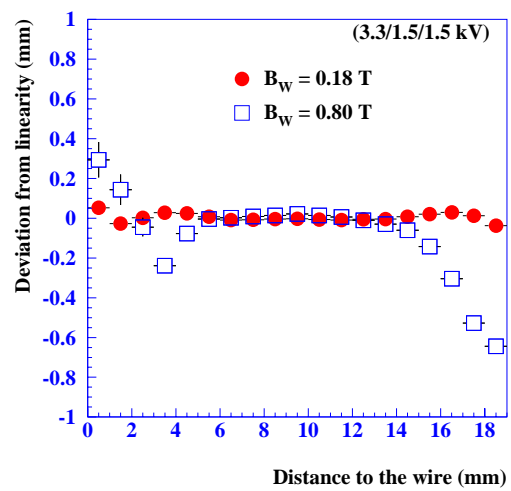


Fig. 6.

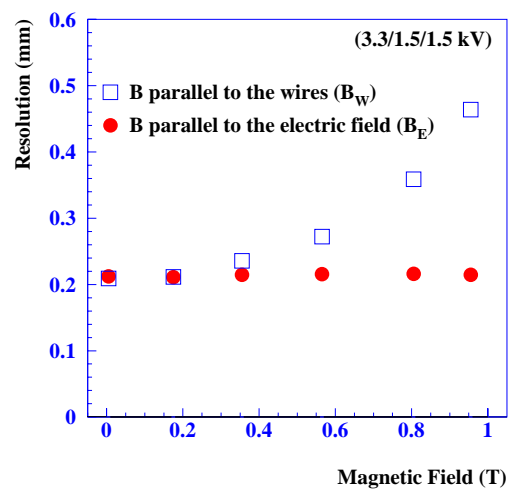


Fig. 7.

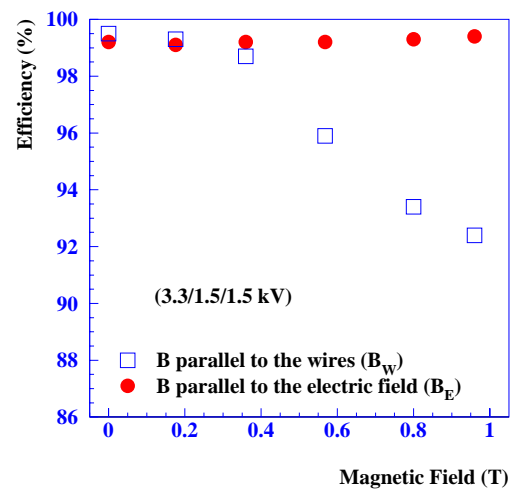


Fig. 8.

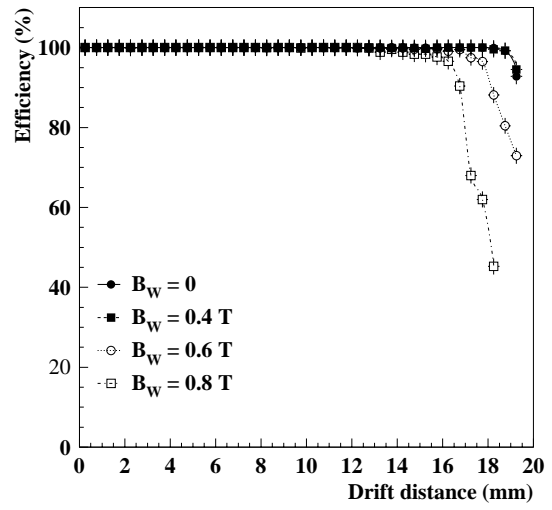


Fig. 9.

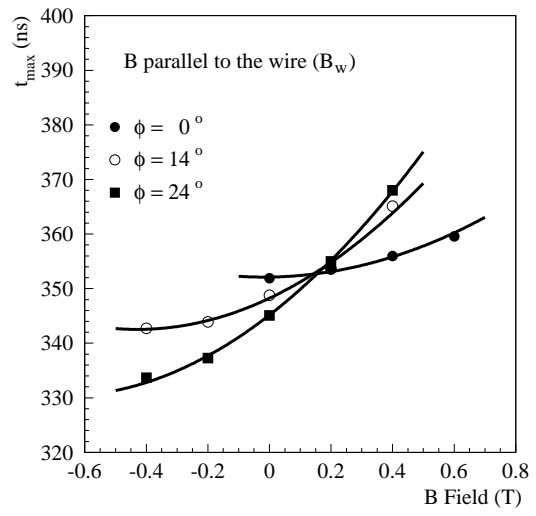


Fig. 10.

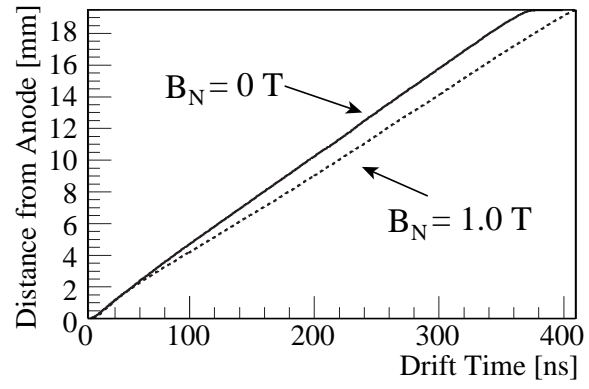


Fig. 11.

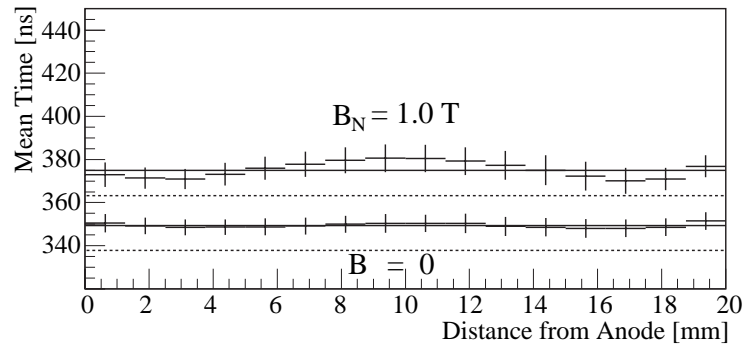


Fig. 12.

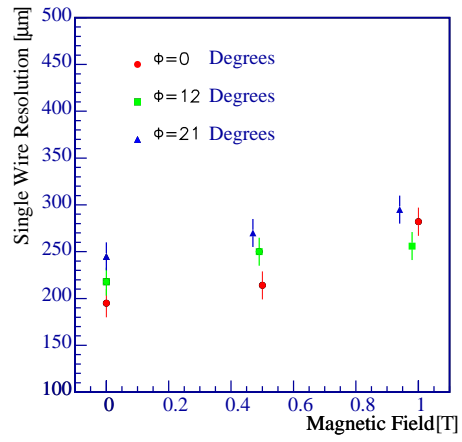


Fig. 13.

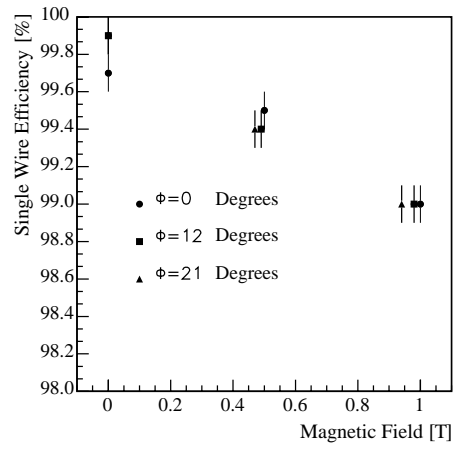


Fig. 14.

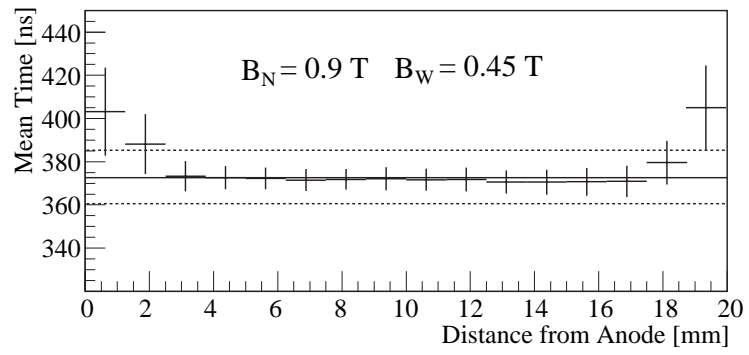


Fig. 15.